Trans-ruthenium(II) complexes for photoactivated cChemotherapy: from design to anticancer activity

Verbeet, W.

Chapter 6

Summary, discussion, and outlook

6.1 Summary

Metallodrugs play a crucial role in modern cancer treatment, with platinum(II)-based drugs being used in about half of all chemotherapeutic regimes prescribed to cancer patients worldwide. Despite their broad application, Pt(II)-drugs suffer from several limitations including systemic toxicity and resistance. The numerous limitations of Pt-drugs have therefore sparked the search for chemotherapeutics based on alternative transition metals, including gold, palladium, iron, or ruthenium. **Chapter 1** provides a general overview of the clinical application of Pt-based and Ru-based anticancer drugs and describes the recent progress made in the development of photoactivated chemotherapy (PACT).

Since polypyridyl ligands are key building blocks in many transition metal-based therapeutics, the necessity for efficient and simple functionalization methods for polypyridyl ligands is high, with synthetic methods evolving constantly. As part of this development, a new synthetic route towards *ortho*-amino-polypyridines is reported in **Chapter 2**. Starting from pyridine *N*-oxides, the described reaction conditions allow for functionalization with one to three amine substituents of various polypyridine derivatives, including bipyridine, phenanthroline, terpyridine, quinoline, and isoquinoline. The simplicity, efficiency and selectivity of this method also allow for easy upscaling, as exemplified by the high-yielding preparation of 2,2'-bipyridine-6-amine at a >66 mmol scale.

The study reported in **Chapter 3** was aimed at investigating the possibility to sequentially photosubstitute two monodentate ligands from a single *trans*-ruthenium(II) polypyridyl complex upon two-color light irradiation. To do so, a series of symmetric complexes was synthesized based on the *trans*-$[Ru(RL)(X)(Y)]^{2+}$ scaffold, where RL is HL (di([2,2'-bipyridin]-6-yl)amine) or MeL (di([2,2'-bipyridin]-6-yl)-*N*-methyl-amine), and with identical axial ligands where X=Y=MTE (methyl(2-thioethanol), ACN (acetonitrile) or Py (pyridine). While all complexes were stable in absence of light, irradiation with blue (435 nm), green (505 nm) or red (625 nm) light resulted in significant differences in photosubstitution kinetics depending on the nature of the axial ligands. Additionally, the photosubstitution quantum yields for several complexes appeared to be wavelength dependent, affording one of a few descriptions of anti-kasha behavior in ruthenium-based photosubstitution reactions. These observations encouraged us to synthesize the dissymmetric complex $[Ru(MeL)(Py)(MTE)]^{2+}$, which was achieved by red light irradiation of $[Ru(MeL)(Py)_2]^{2+}$ in presence of free MTE. Strikingly, selective photosubstitution of the Py ligand took place under red light irradiation of this complex, which allowed for developing a protocol that sequentially substituted first Py with red light followed by MTE using subsequent green light irradiation. These results provided the first example of selective, wavelength–dependent photosubstitution in ruthenium polypyridyl complexes. They also allowed for providing the first quantitative analysis of *trans* effects in the excited triplet states in ruthenium complexes.

Applying the results of **Chapter 3**, the concept of dual-targeting PACT was investigated in **Chapter 4**. To do so, pyridine-based nicotinamide phosophoribosyltransferase inhibitor STF31 and thioether-based microtubule polymerization inhibitor MTI were incorporated in the dissymmetric scaffold reported in **Chapter 3**. The corresponding dissymmetric complexes $[Ru(MeL)(STF31)(MTI)]^{2+}$ and the symmetric analogues $[Ru(MeL)(STF31)_2]^{2+}$ and $[Ru(MeL)(MTI)_2]^{2+}$ were synthesized and characterized. They exhibited distinct photoreactivity upon irradiation with blue, green, or red light in aqueous solution. Importantly, the wavelength-dependent sequential release of both ligands observed in **Chapter 3** was retained in the dissymmetric $[Ru(MeL)(STF31)(MTI)]^{2+}$ complex: releasing STF31 first was possible using red light, followed by MTI using blue light. *In vitro* evaluation of the bis-MTI complex in several human cancer cell lines under both normoxia and hypoxia showed strong dark toxicity but little additional toxicity when activated with green or red light. However, the toxicity of the bis-STF31 and STF31-MTI complexes increased up to 33–fold upon photoactivation with green light. Co-treatment of cells with an equimolar STF31:MTI mixture of both free inhibitors in the same *in vitro* conditions revealed a synergistic effect between the two inhibitors. Strikingly, this synergistic effect was also observed upon green-light activation of the $[Ru(MeL)(STF31)(MTI)]^{2+}$ complex; this observation was independent from the O_2 concentration. The exceptional photochemical and *in vitro* properties of the dissymmetric complex $[Ru(MeL)(STF31)(MTI)]^{2+}$ underline the potential of such dual-targeting PACT compounds, especially for the treatment of hypoxic tumors.

For many PACT compounds reported in the literature, the ruthenium fragment mainly functions as a photocleavable protective group to prevent interaction between an organic cytotoxic inhibitor and its protein target.[1] While this approach has shown great promise in killing cancer cells, it neglects the potential of the photoreleased ruthenium photocage as a potential biologically-active moiety, besides the photoreleased cytotoxic ligand. Although few studies have reported interaction between the ruthenium complexes and nucleic acids, no rationally designed photoactivatable Ru(II)-based protein inhibitors have been reported to date.[2] In **Chapter 5**, two strategies are reported for the design and development of novel PACT compounds targeting Heme Oxygenase 1 (HO-1). The first strategy focused on the modification of the tetrapyridyl ligand di([2,2'-bipyridin]-6-yl)amine (HL) with propyl carboxylic acid groups through cross-coupling or pyridylic C-H functionalization reactions. Upon coordination, the resulting ruthenium(II) complex mimics the natural HO-1 substrate, i.e., heme and as a result inhibit HO-1 after photorelease of the two monodentate, axial ligands. In the second strategy a series of complexes is reported based on $[Ru(MeL)(QC82)(X)]^{2+}$ where QC82 is a known imidazole-based organic inhibitor of HO-1, and X is QC82, pyridine or STF31. While photosubstitution reactions were observed in all complexes upon irradiation with green or red light, a single QC82 ligand remained coordinated in the Ru-photoproduct. To evaluate the HO-1 inhibiting potential of this

ruthenium-containing photoproduct, *in silico* docking studies of $[Ru(MeL)(QC82)]^{2+}$ with HO-1 were performed, which suggested a binding mode similar to that of heme. Although the complexes $[Ru(MeL)(QC82)_2]^{2+}$ and $[Ru(MeL)(QC82)(STF31)]^{2+}$ showed significant *in vitro* cytotoxcicity in human skin melanoma cancer cells, with the currently available data it was impossible to conclude that this cytotoxicity was a consequence of (or related to) HO-1 inhibition. These results do, however, provide a foundation for future development of photoactivatable ruthenium-based HO-1 inhibitors.

6.2 Discussion

6.2.1 Observation of *trans* effects in excited ruthenium(II) complexes

In coordination chemistry the ability of a ligand to labilize the metal-ligand bond in *trans* position, which is called the "*trans* effect", is a widely reported yet poorly understood kinetic phenomenon. Its thermodynamic counterpart, called the *trans* influence, characterizes an elongation of a metal-ligand bond distance in the ground state due to the influence of the *trans* ligand. Both effects are frequently described for square planar complexes containing a d^8 metal center (e.g., Pt(II)) and less for octahedral complexes with a metal center either in d^0 or d^6 electron configuration, such as Ru(II).[3,4] Despite the many reports and decades of research, a conclusive and universal understanding of the underlying mechanisms of the *trans* effect remains to be described.

The preparation of cisplatin often serves as the textbook example of this kinetic effect, where addition of ammonia to tetrachloroplatinate(II) ($[PtCl_4]^{2-}$) results in the formation of cisplatin (*cis*-$[PtCl_2(NH_3)_2]$). This reaction proceeds through the $[PtCl_3(NH_2)]^-$ monosubstituted intermediate, which proceeds forming the final product cisplatin as shown in Figure 6.1A, due to the stronger *trans* effect of Cl^- compared to NH_3. A large number of experimental investigations exploring the effect of the *trans*-ligand on the substitution kinetics of square-planar Pt(II) complexes have led to the following order of ligands with decreasing *trans*-effect:[5]

$$\begin{aligned} &CN^-, CO, NO, C_2H_4 > PR_3, H^-, CH_3^-, SC(NH_2)_2, SR_3 > SO_3H^- \\ &> I^-, SCN^- > Br^- > Cl^- > Py > RNH_2, NH_3 > OH^- > F^- \end{aligned} \quad (6.1)$$

To explain the relative order of *trans*-directing ligands, the reaction mechanism needs to be known. In the case of square-planar Pt(II) complexes, substitution usually occurs through an associative mechanism with the formation of a trigonal bipyramidal transition state as shown in Figure 6.1. Computational studies have confirmed that the *trans*-effect strength correlates with the electronic nature of the *trans* ligand T through both electron donation and back-donation.[5–7] In more detail, σ-donor ligands tend to destabilize the ground state GS (Figure 6.1B) while π-acceptor ligands stabilize the transition state TS (Figure 6.1C).

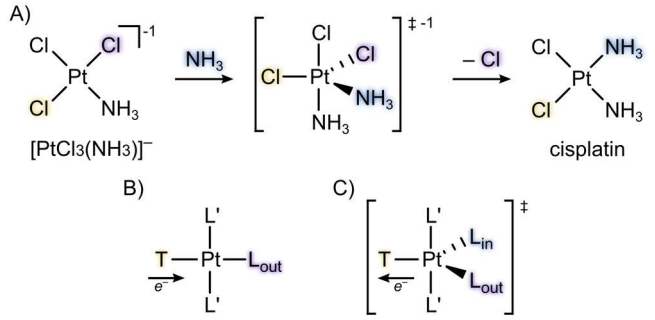

Figure 6.1 The substitution reaction (A) of chloride by ammonia from $[PtCl_3(NH_3)]^-$ forming cisplatin. Schematic representation (B, C) of how the *trans* ligand T can affect the substitution of L_{out} in square-planar Pt(II) complexes. T can either destabilize the ground state GS through electron donation (B) or stabilize the transition state TS through electron withdrawal (C), where L' are spectator ligands, L_{out} is the ligand to be substituted (outgoing) and L_{in} is the substituting ligand (incoming).

The structures and substitution reactions of octahedral complexes are geometrically more complicated than of square planar complexes, in the sense that more isomers may exist both for the reagent and the product. Therefore, the *trans* effect in octahedral complexes has been less studied systematically in the literature. Importantly, ligand substitution in octahedral complexes generally occurs dissociatively rather than associatively as in square planar complexes. The difference in substitution mechanism makes that the *trans* effect and *trans* influence often correlate in octahedral complexes. Although trends have been observed in numerous studies, many exceptions are known and dependent on the metal center, its electron configuration as well as the involved ligands.[4] However, a more recent computational study using conceptual density functional theory has provided a quantitative scale of *trans* effect strength by monitoring differences in electron density of d^6 octahedral complexes.[8] Although the scope of investigated ligands is rather small, the computational results closely matched the experimental ones, indicating that *trans* effects are primarily regulated by the electron-donating properties of the *trans* ligand.

The work presented in this PhD thesis involves the photochemical characterization of multiple Ru(II)-tetrapyridyl complexes containing two photolabile, monodentate ligands in *trans* positions. These monodentate ligands include derivatives of pyridine, thioether, water and N-methyl-imidazole. As observed in the crystal structures of several of these complexes, reported in **Chapter 3** and **Chapter 5**, the ligand-Ru(II) bond lengths are not significantly different upon varying the *trans* ligands, indicating the absence of significant *trans* influence in the ground state of these molecules. Furthermore, at the investigated temperatures these *trans*-Ru(II) polypyridyl complexes only underwent ligand substitution when irradiated with light, limiting the possibilities to study their ground state *trans* effects. However, detailed quantitative analysis of the photosubstitution kinetics reported in this

thesis provides new insights into *trans* effects in the excited states of ruthenium compounds (Table 6.1).

Table 6.1 Quantum yield $\varphi_{\lambda irr}$ and photoreactivity $\zeta_{\lambda irr}$ ($\zeta_{\lambda irr} = \varphi_{\lambda irr} \times \varepsilon_{\lambda irr}$) for the photosubstitution of pyridine from $[Ru(MeL)(L)(Py)]^{2+}$ with different *trans* ligands **L** in aqueous solution.

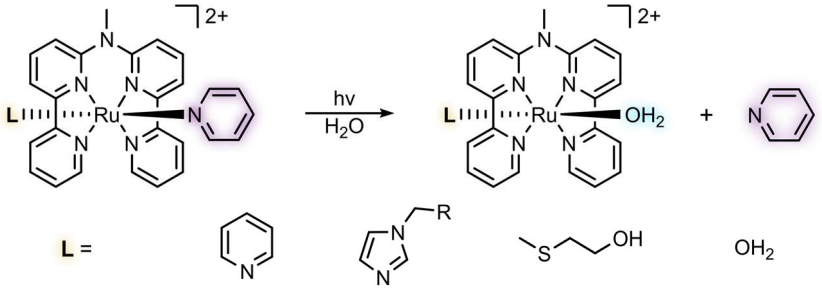

φ_{505}	0.025	0.014	0.019	0.00019
ζ_{505}	110	100	32	1.1
φ_{625}	0.015	0.017	0.014	0.00005
ζ_{625}	0.65	5.6	0.046	0.020

Differences in reaction kinetics between photoactive compounds are generally evaluated by comparing their efficiency to generate a specific excited state or reaction product, i.e., by comparing their photosubstitution quantum yields. Comparing photochemical kinetics based on quantum yields is in many cases preferred as it ignores differences in light absorption properties. Also, this habit is driven by the common assumption that Kasha's rule is valid, which states that once the excited state is obtained the probability to obtain a molecule of photoproduct does not depend too much on the irradiation wavelength, and hence that only quantum yields matter. When examining the photosubstitution kinetics of pyridine from $[Ru(MeL)(L)(Py)]^{2+}$ as shown in Table 6.1, we found that quantum yields for its photosubstitution with red light were highly similar for complexes with different *trans* ligands L = pyridine (Py), N-methyl-imidazole (NMI) or MTE; only for L = water a significant drop of the quantum yield was observed. For green light, the measured differences were slightly more significant and suggested a decreasing kinetic *trans*-effect in the order Py > MTE > NMI >> H_2O.

On the other hand, we found that the photosubstitution quantum yield depended on the irradiation wavelength and hence did not really obey Kasha's rule. In addition, the generation of an excited state through light absorption is a crucial step during any photoreaction, so that the kinetics utterly depend on the absorption of a complex as well. It would hence be more realistic, when comparing photosubstitution kinetics, to compare instead of quantum yields $\varphi_{\lambda\,irr}$ the photochemical reactivities $\zeta_{\lambda\,irr}$, which is defined as the product of the (dimensionless) quantum yield $\varphi_{\lambda\,irr}$ and the molar absorptivity

$\varepsilon_{\lambda\ irr}$ (in $M^{-1}\ cm^{-1}$).When comparing the photochemical reactivities of $[Ru(MeL)(L)(Py)]^{2+}$, the trends at both wavelengths were different from those observed for quantum yields (Table 6.1). Under green light irradiation ζ_{505} decreased in the order NMI > Py > MTE >> H_2O. The differences in ζ_{625} values were way larger than those of the φ_{625} values, highlighting the very different red light absorption of the different molecules. Overall, a *trans* N-methyl-imidazole ligand seems to be the best to labilize a pyridine ligand on this type of ruthenium complexes using red light, both because it increases the photosubstitution quantum yield and because it increases the molar absorption coefficient in this domain of the spectrum. These results emphasize the difficulty of predicting the kinetics of photosubstitution reactions for *trans*-Ru(II) polypyridyl complexes, because one needs to understand not only the distribution and nature of the excited states of the reagent, its light absorption properties, but also the mechanism of the reaction.

Since the photolability of pyridine in $[Ru(MeL)(L)(Py)]^{2+}$ appears to depend on the *trans*-ligand L, the electronic nature of the *trans*-ligand likely affects the energies of the excited states involved in photosubstitution. To qualitatively evaluate these effects, the energies of the frontier molecular orbitals (FMOs) of Py, NMI, MTE and H_2O were calculated with density functional theory (DFT) at the BLYP/def2-svp level using ORCA 6.1 (Figure 6.2).[9] All ligands act as σ donors with an decreasing σ-donating strength following the order MTE > Py ~ NMI >> H_2O. The order follows the decreasing energy level of their highest occupied σ molecular orbital (HOMO): assuming that the empty metal-based d-orbitals on ruthenium are high in energy, they will interact more strongly with monodentate ligands that have a higher HOMO (if symmetry allows). In addition, Py and NMI contain an aromatic system and a low-lying lowest unoccupied molecular orbital (LUMO) with an anti-bonding π* character that can interact with filled d-orbitals of the metal center (back-bonding). However, the additional mesomeric N-donor atom in NMI increases the electron density of the π system and thereby the energy of its π* LUMO, thus making it a worse π-acceptor than Py. Similarly, the higher HOMO-2 of π character of NMI also increase its π-donating abilities compared with Py. In contrast, the coordinating sulfur atom in MTE is sp^3 hybridized and has an anti-bonding LUMO orbital of σ* character that could accept electrons from the metal via a π-like overlap, but this interaction is energetically unfavorable as the LUMO is relatively high in energy. While one S-based electron pair acts as a σ donor (HOMO) in a "side-on" binding mode, the second electron pair is located in a low-lying occupied π orbital (HOMO-2), resulting in weak π-donation to the metal center. Finally, H_2O has the lowest σ donating properties and little to no π-accepting properties. According to this analysis Py is an average σ-donating and the best π-acceptor ligand in the series, NMI an equally good σ-donor but less π-accepting ligand, while MTE is the strongest σ-donor and a weak

σ*-acceptor and π-donor, and finally H_2O is the weakest σ-donating ligand with no π-accepting or π-donating properties.

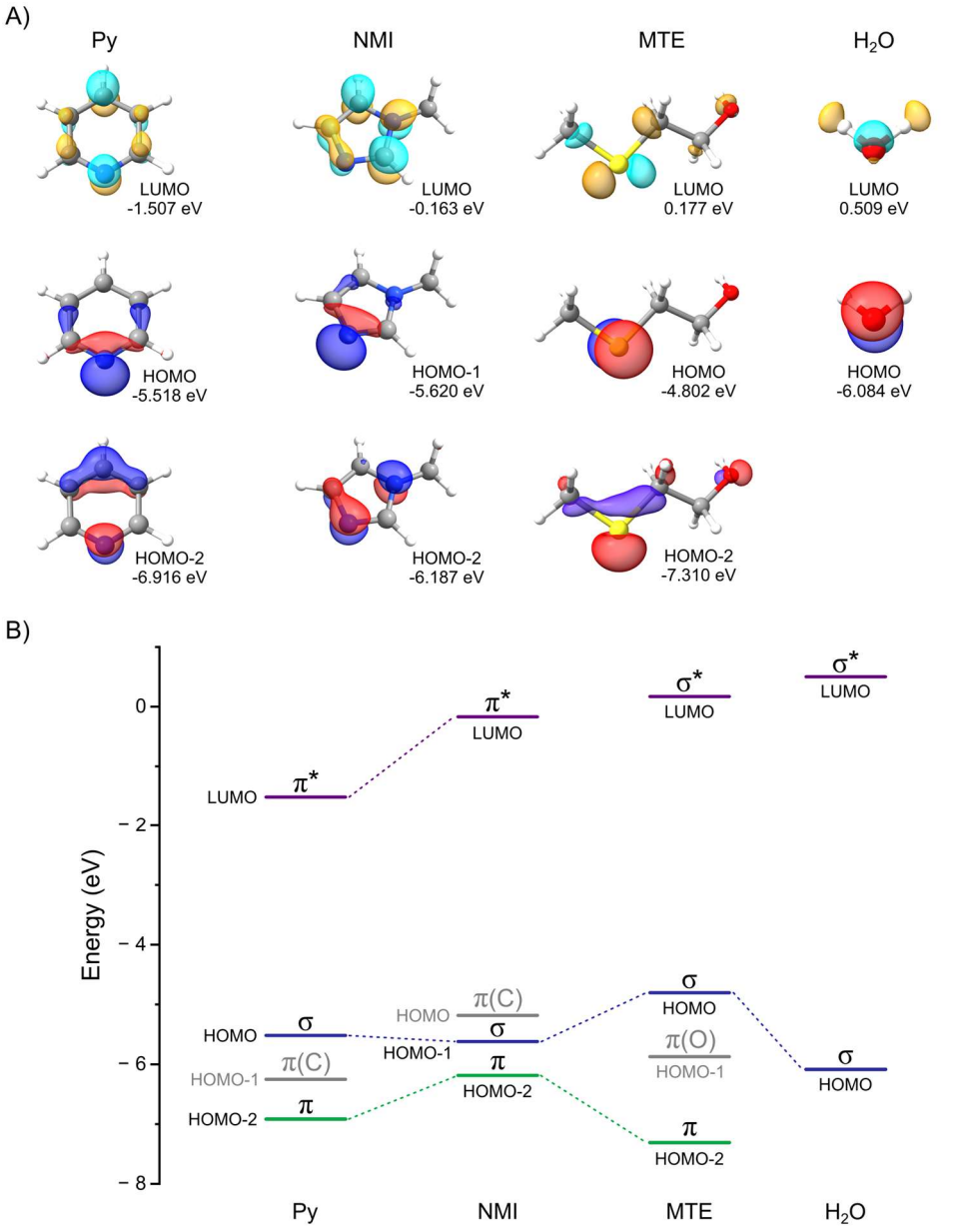

Figure 6.2: Comparison between the frontier molecular orbitals (A) and corresponding energies (B) of Py, NMI, MTE, and water. Calculated with density functional theory using the Becke-Lee-Yang-Parr (BLYP) functional with def2-svp basis set in the ORCA 6.1 software package.[9]

This qualitative orbital analysis highlights the fundamental differences in electronic character of the different monodentate ligands in this series, but it does not allow us to fully rationalize the *trans* effects in the triplet excited state. If we assume that green light quantum yields offer the best measure of this photo-*trans* effect, then the decrease in *trans*-effect in $[Ru(MeL)(L)(Py)]^{2+}$ complexes follows Py > MTE > NMI >> H_2O, which more or less follows the ligand-field strength of the *trans* ligand in the traditional spectrochemical series.[10] If we focus on red light and compare ζ_{625} values, then the *trans* effect decreases following NMI > Py > MTE >> H_2O, which does not follow the spectrochemical series notably due to the effect of the *trans* ligand on the absorption spectrum of the complex. While the FMO analysis provides qualitative insight into the electronic nature of the ligands, it must be noted that these FMOs will likely differ upon coordination to a metal center. In fact, the properties of the free *trans* ligands cannot be used to directly predict their effect on the dynamics of the excited state of the metal complex, which depends on the spectator ligands, on the geometry and sterics of the Ru(II) complex, on the solvent, and finally, on the irradiation wavelength.

The observed increase in photosubstitution kinetics with stronger donating ligands in *trans* position is consistent with trends reported by others. For example in the ground state albeit with a different mechanism, the rate of H_2O substitution by acetonitrile was reported to increase with increasing electron-donating strength of substituent X in $[Ru(tpy)(4,4'\text{-}X_2bpy)(H_2O)]^{2+}$ complexes, with tpy = 2,2':6',2"-terpyridine, 4,4'-X_2bpy = 4,4'-bis-substituted 2,2'-bipyridine and substituent X = H, CH_3, OCH_3, NH_2 and $N(CH_3)_2$.[11] Similarly, the photosubstitution quantum yield of acetonitrile in aqueous solution increased with the electron-donating ability of R in $[Ru(R\text{-}phtpy)(acac)(MeCN)]^{+}$, where acac = acetylacetonate and R-phtpy = 4'-(4-R-phenyl)-2,2':6',2"-terpyridine with R = $N(ethyl)_2$, $N(CH_3)_2$, OCH_3, CH_3, H, or NO_2.[12] This effect on the photosubstitution of acetonitrile in aqueous solution was also reported by the Turro group for $[Ru(tpy)(4,4'\text{-}X_2bpy)(L)]^{2+}$, where X = H, CH_3, OCH_3, or *t*-$C(CH_3)_3$ and L = acetonitrile.[13] However, for the pyridine analogues of these complexes (L = pyridine), photosubstitution in aqueous solution occurred very inefficiently when irradiated with green light (500 nm; $\varphi < 0.0001$), pointing to the very band *trans* effect of the *trans* pyridine ring of the bpy chelate in this family of complexes. Interestingly, both the acetonitrile and pyridine complexes showed an increasing energy gap between the ^{3}MLCT and ^{3}MC states upon increasing donating strength of the bidentate ligand. This observation led to the controversial conclusion that the photo-release of acetonitrile must occur directly from the ^{3}MLCT state, without thermal promotion to the ^{3}MC state. Together with our findings, these contradicting reports indicate that the mechanism of photosubstitution may be strongly depend on the nature of the released ligand; they also highlight the complex photochemistry behind photosubstitution reactions. In absence of a full mechanistic understanding of photosubstitution, providing a concluding interpretation of experimental trends in excited state *trans* effects remains challenging.

More elaborate computational approaches may be needed, such as the dynamic model described recently by our group.[14]

6.2.2 Determining the (photo)toxicity of dual-targeting ruthenium(II) complexes

One of the important aspects for ruthenium(II) complexes to be effective as a PACT compound is the difference in cytotoxicity of the intact complex in the dark and the combined cytotoxicity of the photoproducts released by light activation. Several complexes reported in **Chapter 4** and **Chapter 5** can release two biologically active ligands and therefore, an intermediate is formed during light activation. Although the light-dose needed to ensure a photo-stationary state *in vitro* was determined, formation of this intermediate is unavoidable and may give rise to unexpected biological effects. For example, in **Chapter 5** the intermediate $[Ru(MeL)(QC82)(H_2O)]^{2+}$ obtained upon release of STF31 from $[Ru(MeL)(QC82)(STF31)]^{2+}$ was found to be a promising inhibitor for HO-1 (according to *in silico* results). In **Chapter 4**, the Ru-MTI intermediate $[Ru(MeL)(MTI)(H_2O)]^{2+}$ obtained after release of STF31 from $[Ru(MeL)(STF31)(MTI)]^{2+}$ may also interact with biological off-targets, either related to the ligand that remains coordinated or via the free coordination site on the Ru(II) center. While the biological effects of such reactive species are not expected, they could be beneficial for eradicating cancer cells.

Clinically evaluated Ru(II)-based anticancer drug BOLD-100 owes its success to multiple modes-of-action due to thermal ligand exchange with biomolecules, resulting in a potentially large number of bioinorganic interactions that make resistance mechanisms difficult to evolve. A similar mechanism could occur for the bis-aqua complexes or mono-aqua complexes obtained from light-activated $[Ru(MeL)(QC82)(STF31)]^{2+}$ or $[Ru(MeL)(STF31)(MTI)]^{2+}$, although the results obtained so far do not suggest such behavior. To evaluate such potential behaviour of the complexes presented here, $[Ru(MeL)(Py)(MTE)]^{2+}$ was incorporated in the cytotoxicity evaluation reported in **Chapter 4**. The lack of toxicity observed for this model complex with or without light irradiation could, however, be due to its hydrophilicity, which predicts lower cellular uptake compared with the complexes bound to more hydrophobic inhibitors STF31 and MTI.

Alternatively, drug-ruthenium conjugates may interact with biomolecules prior to activation. Such unexpected behavior was encountered in a study reported by Toupin et al., in which a Ru(II)-caged inhibitor of cytochrome P450 3A4 was investigated.[15] Surprisingly, the Ru(II)-inhibitor conjugate exhibited a stronger inhibitory effect than the free inhibitor. Crystal structure analysis of the enzyme bound to the Ru(II)-inhibitor complex showed that the conjugate interacted with a hydrophobic pocket close to the catalystic site of the enzyme. This unexpected binding mode was different from that of the parent organic inhibitor, which exemplifies how unexpected the interaction between Ru(II)-based complexes and proteins can be.

While the complexes reported here have been shown to reduce cancer cell proliferation after light activation, the presented data do not provide evidence for inhibition of the targeted proteins. *In vitro* inhibition assays for NAMPT and microtubule polymerization are commercially available, but a lack of time prevented verification of the expected inhibition properties.[16,17] Proving inhibition of HO-1, however, remains more challenging because no commercial *in vitro* assays are available, and the published chemical assay could not be reproduced in our labs. Therefore, biological evaluation of HO-1 inhibition may be preferred and is typically performed by monitoring the enzyme's activity from isolated animal samples such as microsomal extracts from rat spleen.[18]

6.3 Outlook

The results reported in this thesis provide a proof-of-concept for dual-targeting PACT compounds from which two different biologically active ligands can be released sequentially. To further develop this strategy and rationally design new compounds, the exact photochemical mechanisms need to be elucidated with a focus on understanding *trans* effects in the excited state of coordination compounds. Combination of time-resolved spectroscopic techniques with time-dependent density functional theory (TD-DFT) could greatly advance the understanding of these complex systems. A likely first step would be to compare lifetimes of the different triplet excited states and to determine their electronic nature (i.e., whether they are MLCT or MC states). Besides further characterization of the complexes reported in this thesis, extending the series based on $[Ru(MeL)(L)(Py)]^{2+}$ with other monodentate ligands L following the ligand FMO analysis should provide valuable insights (Figure 6.3). Firstly, incorporating pyridyl ligands containing electron-withdrawing substituents could provide insight into the effect of increasing π-accepting character on the photosubstitution kinetics of Py in $[Ru(MeL)(L)(Py)]^{2+}$. For example, the LUMO energy of 4-(trifluoromethyl)pyridine is lower than that of Py, making it a better π-acceptor while maintaining a similar energy gap between HOMO and HOMO-2 of the ligand. On the other hand, pyridyl ligands containing electron-donating substituents such as 4-(methoxy)pyridine, result in increased σ-donation and π-donation similar to that of NMI, as shown in Figure 6.2. In **Chapter 3**, the preparation and photochemical characterization of acetonitrile-containing symmetric complex $[Ru(MeL)(ACN)_2]^{2+}$ is described. While this complex appeared to be too reactive for the preparation of a dissymmetric complex, further efforts could provide highly photoreactive complexes with strong *trans* effects due to the low-lying HOMO orbitals of ACN. Similar to the FMOs of MTE, trimethylphosphine (PMe_3) is a relatively strong σ–donor due to the high-lying HOMO orbital while the high-lying LUMO makes π back-donation from the Ru(II) center unlikely. The steric bulk of PMe_3 also makes it an interesting candidate to investigate the role of sterics on excited-state *trans* effects. Lastly, use of primary amines such as n-butylamine that are primarily σ–donors could

provide insight in the effects of ligands that coordinate to Ru(II) without the participation of π-orbitals. Importantly, the non-conventional photochemical synthetic route towards the dissymmetric complexes reported in this thesis is far from straightforward and difficult to upscale. Further optimization will be required to synthetically access novel dissymmetric ruthenium compounds bearing various monodentate ligands beyond those reported in this thesis.

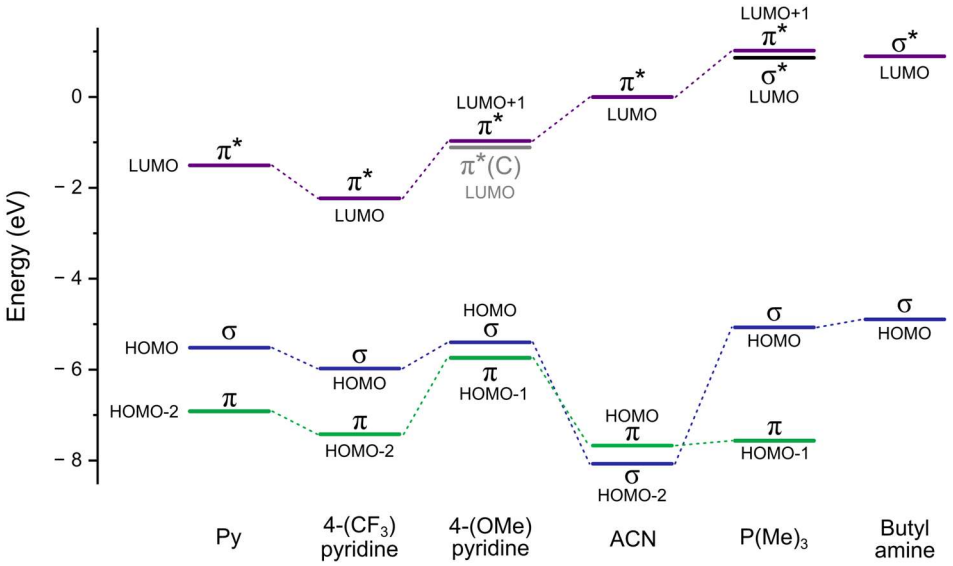

Figure 6.3 Comparison of the frontier molecular orbital energies of Py, 4-(trifluoromethyl)pyridine, 4-(methoxy)pyridine, ACN, trimethylphosphine and 1-butylamine. Calculated with density functional theory using the Becke-Lee-Yang-Parr (BLYP) functional with def2-svp basis set in the ORCA software package.[9]

To further improve the anticancer efficacy of dual-targeting PACT compounds, several aspects can be considered (Figure 6.4). Firstly, the STF31/MTI combination reported in **Chapter 4** was found to work synergistically, while synergism had not been reported for this combination before. Incorporating a combination that is known to induce synergy could therefore induce an even stronger inhibitory effect on cancer cell proliferation after photo-activation.[19] Secondly, the dissymmetric complex $[Ru(MeL)(STF31)(MTI)]^{2+}$ releases the two biologically active ligands, but also a Ru(II)-based photoproduct for which no significant cytotoxicity was observed. Increasing the toxicity of this Ru(II)-based photoproduct could therefore add another dimension to the anticancer properties of the overall complex. A possible strategy to increase its toxicity could be to extend the aromatic π surface of the tetrapyridyl ligand, which has been shown to result in Ru(II) complexes with PDT characteristics and DNA-binding properties.[20,21] Since several precursors of such extended polypyridyl ligands have been reported in **Chapter 2**, the preparation of such

complexes might be relatively straightforward. Alternatively, covalently linking a third drug to the bridging nitrogen in the tetrapyridyl ligand could also lead to a toxic, Ru-based photoproduct. Apart from phototoxicity of the compounds, high accumulation in a specific tissue, cell type or organelle is a desirable characteristic in anticancer therapeutic compounds. Combining a targeting moiety into the dual-targeting PACT strategy would therefore be of great interest as it has been shown to benefit PACT.[22] In the molecule shown in Figure 6.4, both drug 2 or drug 3 could be tumor-targeting fragments. The vast range of design possibilities makes the multifunctional ruthenium platform presented in this thesis a promising and tunable scaffold for bioinorganic applications in oncology.

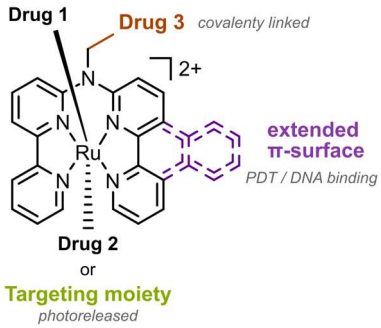

Figure 6.4 General design strategy towards the next generation of dual-targeting PACT compounds.

6.4 References

(1) Bonnet, S. *J. Am. Chem. Soc.* **2023**, *145* (43), 23397–23415.
(2) Papish, E. T.; Oladipupo, O. E. *Current Opinion in Chemical Biology* **2022**, *68*, 102143.
(3) Quagliano, J. V.; Schubert, Leo. *Chem. Rev.* **1952**, *50* (2), 201–260.
(4) Coe, B. J.; Glenwright, S. J. *Coordination Chemistry Reviews* **2000**, *203* (1), 5–80.
(5) Chval, Z.; Sip, M.; Burda, J. V. *J Comput Chem* **2008**, *29* (14), 2370–2381.
(6) Pinter, B.; Van Speybroeck, V.; Waroquier, M.; Geerlings, P.; De Proft, F. *Phys. Chem. Chem. Phys.* **2013**, *15* (40), 17354.
(7) Santos-Jr, C. V.; Da Silva, G. M. B.; Dias, R. P.; Moura, R. T.; Da Silva, J. C. S. *Advcd Theory and Sims* **2024**, *7* (5), 2301148.
(8) Guégan, F.; Tognetti, V.; Joubert, L.; Chermette, H.; Luneau, D.; Morell, C. *Phys. Chem. Chem. Phys.* **2016**, *18* (2), 982–990.
(9) Neese, F. *WIREs Comput Mol Sci* **2025**, *15* (2), e70019.
(10) Ishii, T.; Tsuboi, S.; Sakane, G.; Yamashita, M.; Breedlove, B. K. *Dalton Trans.* **2009**, No. 4, 680–687.
(11) Mecchia Ortiz, J. H.; Peyrot, A. M.; Fagalde, F.; Katz, N. E. *Inorganic Chemistry Communications* **2018**, *98*, 44–47.
(12) Mudrak, V.; Lacroix, P. G.; Labra-Vázquez, P.; Tassé, M.; Mallet-Ladeira, S.; Malfant, I. *Dalton Trans.* **2025**, *54* (22), 9021–9031.
(13) Dunbar, M. N.; Steinke, S. J.; Piechota, E. J.; Turro, C. *J. Phys. Chem. A* **2024**, *128* (3), 599–610.
(14) Hakkennes, M. L. A.; Regeni, I.; Husiev, Y.; Andreeva, V. D.; Siegler, M. A.; Buda, F.; Bonnet, S. *J. Am. Chem. Soc.* **2025**, *147* (39), 35767–35787.

(15) Toupin, N.; Steinke, S. J.; Nadella, S.; Li, A.; Rohrabaugh, T. N.; Samuels, E. R.; Turro, C.; Sevrioukova, I. F.; Kodanko, J. J. *J. Am. Chem. Soc.* **2021**, *143* (24), 9191–9205.
(16) Bretin, L.; Husiev, Y.; Ramu, V.; Zhang, L.; Hakkennes, M.; Abyar, S.; Johns, A. C.; Le Dévédec, S. E.; Betancourt, T.; Kornienko, A.; Bonnet, S. *Angew Chem Int Ed* **2024**, *63* (5), e202316425.
(17) Wang, X.; Xu, T.-Y.; Liu, X.-Z.; Zhang, S.-L.; Wang, P.; Li, Z.-Y.; Guan, Y.-F.; Wang, S.-N.; Dong, G.-Q.; Zhuo, S.; Le, Y.-Y.; Sheng, C.-Q.; Miao, C.-Y. *Sci Rep* **2015**, *5* (1), 12657.
(18) Virzì, N. F.; Alvarez-Lorenzo, C.; Concheiro, A.; Consoli, V.; Salerno, L.; Vanella, L.; Pittalà, V.; Diaz-Rodriguez, P. *International Journal of Pharmaceutics* **2025**, *668*, 124997.
(19) You, T.; Wang, L.; Wang, J.; Xu, D.; Xu, X.; Li, N.; Li, M. J.; Wang, H.; Dong, X. *Sci Data* **2025**, *12* (1), 1284.
(20) Toupin, N. P.; Nadella, S.; Steinke, S. J.; Turro, C.; Kodanko, J. J. *Inorg. Chem.* **2020**, *59* (6), 3919–3933.
(21) Brabec, V.; Kasparkova, J. *Coordination Chemistry Reviews* **2018**, *376*, 75–94.
(22) Zhang, L.; Wang, P.; Zhou, X.-Q.; Bretin, L.; Zeng, X.; Husiev, Y.; Polanco, E. A.; Zhao, G.; Wijaya, L. S.; Biver, T.; Le Dévédec, S. E.; Sun, W.; Bonnet, S. *J. Am. Chem. Soc.* **2023**, *145* (27), 14963–14980.